Inorganic Chemistry

Article

pubs.acs.org/IC

Magnetic Coupling and Slow Relaxation of Magnetization in Chain-Based Mn^{II}, Co^{II}, and Ni^{II} Coordination Frameworks

Jian-Yong Zhang, Kun Wang, Xiu-Bing Li, and En-Qing Gao*

Shanghai Key Laboratory of Green Chemistry and Chemical Processes, Department of Chemistry, East China Normal University, Shanghai 200062, China

Supporting Information

ABSTRACT: Three isomorphous coordination polymers based on the chain with triple $(\mu\text{-}1,1\text{-}N_3)(\mu\text{-}1,3\text{-}COO)_2$ bridges have been synthesized from a new zwitterionic dicarboxylate ligand [L^- = 1-(4-carboxylatobenzyl)pyridinium-4-carboxylate]. They are of formula $[M(L)(N_3)]_n \cdot 3nH_2O$ [M = Mn^{II}, Co^{II}, and Ni^{II}]. In these compounds, the mixed-bridge chains are linked into 2D coordination networks by the *N*-benzylpyridinium spacers. The magnetic properties depend strongly on the nature of the metal center. The magnetic coupling through $(\mu\text{-}1,1\text{-}N_3)(\mu\text{-}1,3\text{-}COO)_2$ is antiferromagnetic in the Mn^{II} compound but ferromagnetic in the Co^{II} and Ni^{II} analogues. Magnetostructural analyses indicate that the magnitude of the magnetic coupling can be correlated to the M−N−M angle of the azide bridge and the average M−O−C−O torsion angle of the carboxylate bridge. As the values of these parameters increase, the antiferromagnetic coupling for Mn^{II} decreases while the ferromagnetic coupling for Co^{II} increases. With strong magnetic anisotropy, the Co^{II} compound behaves as a single-chain magnet showing hysteresis and Glauber-type slow dynamics probably in the infinite-chain region, with Δ_τ/k = 86 K, Δ_ξ/k = 26 K, and Δ_A/k = 34 K. With weaker anisotropy, the Ni^{II} species shows slow relaxation of magnetization at much lower temperature.

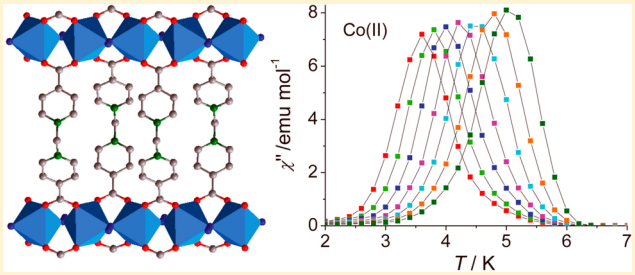

INTRODUCTION

Magnetic studies on molecular systems derived from paramagnetic metal ions have been of interest for decades at the frontier between chemistry and physics, aimed at unveiling new magnetic phenomena, establishing magnetostructural correlations, and obtaining functional molecular materials with potential applications. Following the long-range-ordered molecular magnets[1] and single-molecule magnets (SMMs)[2,3] extensively studied since 1980s and 1990s, respectively, single-chain magnets (SCMs) have emerged as an new active topic of research at the frontier since the first experimental observation of the magnet-like behaviors of magnetically isolated 1D systems a decade ago.[4] It has been established that the design of SCMs requires control of three essential ingredients:[5] (i) a noncanceling spin arrangement along the chain, which can be ferromagnetic (FO), ferrimagnetic (FI), or canted antiferromagnetic (AF) and requires judicious selection of spin carriers and bridging ligands; (ii) a significant uniaxial anisotropy, which can be achieved by employing anisotropic metal ions as spin carriers; (iii) sufficiently weak interchain interactions to ensure 1D dynamics. Chemists have synthesized a number of systems meeting these requirements and proposed a few synthetic approaches toward specific chemical systems with variable structural and magnetic parameters,[5,6] but the rational design of new SCMs is still a great challenge for lack of knowledge of the underlying magnetostructural correlations.

Azide and carboxylate show great versatility and diversity in bridging metal ions and transmitting magnetic coupling, and they are among the most extensively used bridges in the construction of molecular magnetic systems.[7] In particular, a few homospin SCMs with azide or carboxylate bridges have been obtained in the past decades,[8,9] but the versatility and diversity of the bridges cause great difficulties in the rational design of magnetically isolated chains. Recently, we have demonstrated that the use of zwitterionic pyridiniumcarboxylate ligands, in comparison with the usual anionic carboxylates, is an efficient synthetic approach toward 1D coordination motifs with simultaneous μ-1,3-carboxylate and μ-1,1-azide bridges.[10] Furthermore, benefiting from the FO interactions through the simultaneous bridges between anisotropic metal ions, the approach has led to a few homospin Co^{II} and Fe^{II} SCMs,[11] including some interesting systems that exhibit solvent-modulated SCM behaviors and the coexistence of antiferromagnetism, metamagnetism, and SCM dynamics. In a continuation of the research, here we present a systematic study on the synthesis, structure, and magnetic properties of three compounds of formula $[M(L)(N_3)]_n \cdot 3nH_2O$ [M = Mn for **1**, Co for **2**, and Ni for **3**; L^- = 1-(4-carboxylatobenzylpyridinium-4-carboxylate; Chart 1). The three isomorphic compounds consist of 2D coordination networks, in which 1D coordination chains with triple $(\mu\text{-}1,1\text{-}N_3)(\mu\text{-}1,3\text{-}COO)_2$ bridges are interlinked by the L^- spacers. Compound **1** exhibits typical 1D antiferromagnetism, while **2** and **3** display intrachain FO

Received: June 17, 2014
Published: August 19, 2014

   dx.doi.org/10.1021/ic5014279 | *Inorg. Chem.* 2014, 53, 9306−9314

Chart 1. 1-(4-Carboxylatobenzyl)pyridinium-4-carboxylate Ligand (L^-)

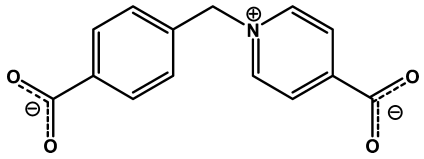

interactions. **2** behaves as an SCM, and **3** also shows slow relaxation of magnetization dynamics and single-chain-based slow dynamics. Comparisons of these compounds with previous analogues have afforded some information on magnetostructural correlations.

EXPERIMENTAL SECTION

Physical Measurements. Elemental analyses (EA) were determined on an Elementar Vario ELIII analyzer. The Fourier transform infrared spectra were recorded in the range 500−4000 cm^{-1} using KBr pellets on a Nicolet NEXUS 670 spectrophotometer. Thermogravimetric analyses (TGA) were carried out on a Mettler Toledo TGA/SDTA851 instrument under flowing air at a heating rate of 5 °C/min. Temperature- and field-dependent magnetic measurements were carried out on a Quantum Design SQUID MPMS-5 magnetometer. Diamagnetic corrections were made with Pascal's constants. Powder X-ray diffraction (PXRD) was recorded on a Rigaku Ultima IV X-ray diffractometer equipped with a Cu-target tube at 35 kV and 25 mA and a graphite monochromator. The reflections of **3** were indexed in the same space group as that determined for **1** and **2** by single-crystal crystallography (vide infra), and the unit cell parameters were refined by the Pawley method using the Reflex module implemented in the *Materials Studio* software,[12] with the data of **2** as the initial values. The final Pawley refinement including the pseudo-Voigt peak-shape profile parameters, the 20-term background polynomials, the Rietveld asymmetry correction parameters, and the Bragg−Brentano zero-point shift parameter gave a satisfactory R_{wp} value of 6.66%. The calculated and experimental PXRD patterns are compared in Figure S1 in the Supporting Information.

Synthesis. All of the reagents and solvents employed were commercially available and supplied without further purification. The ligand 1-(4-carboxybenzyl)pyridinium-4-carboxylate (HL) was prepared according to the literature.[13]

Caution! *Although not encountered in our experiments, azide compounds of metal ions are potentially explosive. Only a small amount of the materials should be prepared, and it should be handled with care.*

*$[Mn(L^2)(N_3)]_n·3nH_2O$ (**1**).* Crystals of **1** were obtained by slow diffusion in an H-shaped tube. An aqueous solution (3 mL) containing HL (0.10 mmol, 0.020 g) and NaN_3 (0.20 mmol, 0.013 g) was added to an arm of the H-shaped tube and a solution of $MnCl_2·4H_2O$ (0.10 mmol, 0.020 g) in the same solvent (3 mL) to the other arm, and then about 15 mL of ethanol was carefully added until the bridge of the tube was filled. Slow diffusion between the two solutions afforded rod-shaped orange crystals of **1** within 1 week, which were washed with water and ethanol and dried in air. Yield: 59%. The phase purity of the bulk product was confirmed by PXRD experiments. Elem anal. Calcd for $C_{14}H_{16}N_4O_7Mn$ (M = 407.24): C, 41.29; H, 3.96; N, 13.76. Found: C, 40.84; H, 3.94; N, 13.67. Main IR (KBr, cm^{-1}): 3444br, 3113m, 3049m, 2964w, 2071vs, 1624vs, 1562vs, 1456m, 1392vs.

*$[Co(L^2)(N_3)]_n·3nH_2O$ (**2**).* The preparation of compound **2** is similar to that of **1**, except that $MnCl_2·4H_2O$ was replaced by $CoCl_2·6H_2O$ (0.10 mmol, 0.024 g). Rod-shaped brown crystals were isolated in a yield of 65%. The phase purity of the bulk product was also confirmed by PXRD experiments. Elem anal. Calcd for $C_{14}H_{16}N_4O_7Co$ (M = 411.24): C, 40.89; H, 3.92; N, 13.62. Found: C, 40.79; H, 4.02; N, 13.44. Main IR (KBr, cm^{-1}): 3437br, 3118w, 3053m, 2964w, 2071vs, 1620vs, 1564s, 1460w, 1394vs.

*$[Ni(L^2)(N_3)]_n·3nH_2O$ (**3**).* The preparation of compound **3** is similar to that of **1**, except that $MnCl_2·4H_2O$ was replaced by $NiCl_2·6H_2O$ (0.10 mmol, 0.024 g). Polycrystalline yellow-green precipitate was isolated after about 3 days. Yield: 54%. All attempts to get single crystals of **3** by different methods were in vain. The phase purity of the bulk product was confirmed by PXRD experiments. Elem anal. Calcd for $C_{14}H_{16}N_4O_7Ni$ (M = 410.99): C, 40.91; H, 3.92; N, 13.63. Found: C, 40.57; H, 4.22; N, 13.39. Main IR (KBr, cm^{-1}): 3446br, 3118w, 3053w, 2966w, 2073vs, 1616s, 1564s, 1460w, 1396vs.

X-ray Crystallography. Diffraction intensity data of **1** and **2** were collected at 296 K on a Bruker APEX II diffractometer equipped with a CCD area detector and graphite-monochromated Mo Kα radiation (λ = 0.71073 Å). Empirical absorption corrections were applied using the *SADABS* program.[14] The structures were solved by direct methods and refined by the full-matrix least-squares method on F^2, with all non-hydrogen atoms refined with anisotropic thermal parameters.[15] All of the hydrogen atoms attached to carbon atoms were placed in calculated positions and refined using the riding model. The hydrogen atoms of the water molecules cannot be located because of the heavy disorder of the guest molecules. The hydrogen atoms have been included in the reported formulas. The orthorhombic *Imma* group imposes C_{2v} point symmetry on the L^- ligand, so the pyridyl nitrogen atom (N4) and one (C5) of the benzene carbon atoms were refined to occupy the same crystallographic position with the same displacement parameters and bisected occupancy factors. A summary of the crystallographic data, data collection, and refinement parameters is provided in Table 1.

Table 1. Crystallographic Data and Structure Refinement Parameters for Compounds 1 and 2

	1	2
empirical formula	$C_{14}H_{16}N_4O_7Mn$	$C_{14}H_{16}N_4O_7Co$
fw	407.25	411.24
cryst syst	orthorhombic	orthorhombic
space group	*Imma*	*Imma*
a, Å	7.3498(15)	7.1400(18)
b, Å	13.692(3)	13.503(4)
c, Å	18.208(4)	18.308(5)
V, Å^3	1832.3(6)	1765.0(8)
Z	4	4
ρ_{calcd}, g cm^{-3}	1.476	1.548
μ, mm^{-1}	0.763	1.017
θ range collected	1.86−26.00	2.22−26.01
data/unique	4057/1019	4848/987
R_{int}	0.0447	0.0319
S on F^2	1.046	1.030
R1, wR2 [$I > 2\sigma(I)$]	0.0590, 0.1628	0.0458, 0.1272
R1, wR2 (all data)	0.0649, 0.1678	0.0554, 0.1351

RESULTS AND DISCUSSION

Description of the Crystal Structures. Single-crystal X-ray structure analysis revealed that compounds **1** and **2** are isomorphous, crystallizing in the *Imma* space group and exhibiting 2D coordination networks (Figure 1). The asymmetric unit of the structure is only $^1/_4$ of the formula. The metal ion resides at a crystallographic 2/*m* position and assumes the *trans*-octahedral $[N_2O_4]$ coordination geometry completed by four equivalent carboxylate O1 atoms and two equivalent azide N1 atoms. The Mn−N/O bond distances 2.215(3)/2.169(3) Å for **1** are longer than Co−N/O for **2** [2.109(3)/2.091(2) Å]. Neighboring M^{II} ions are triply bridged by two carboxylate groups in the *syn,syn*-μ-1,3 mode and an azide ion in the end-on μ-1,1 mode to generate a 1D uniform $[M(N_3)(OCO)_2]_n$ chain along the *a* direction. The M···M distances spanned by the triple bridges are 3.675(1) Å for **1** and

dx.doi.org/10.1021/ic5014279 | Inorg. Chem. 2014, 53, 9306−9314

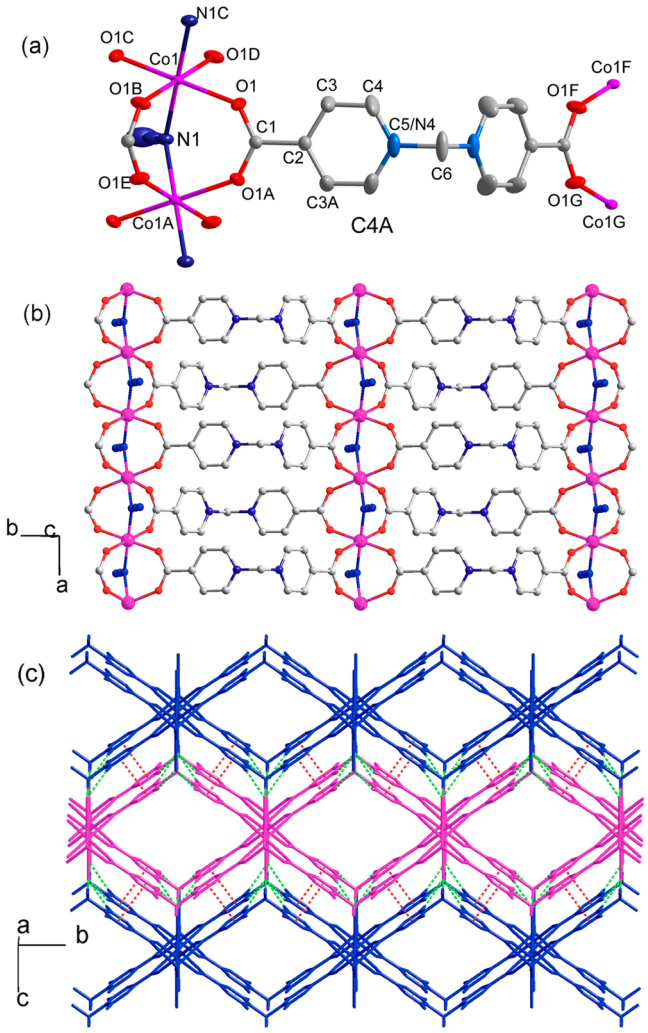

Figure 1. Structure of **2**. (a) Coordination environments of the metal ion and ligands. Thermal ellipsoids were drawn at the 30% probability level, and the C5 and N4 atoms are located at the same crystallographic positions with equal occupancy factors. Symmetry code: A = $-x, y, z$; B = $x, -y + {}^{3}/_{2}, z$; C = $-x + {}^{1}/_{2}, -y + {}^{3}/_{2}, -z + {}^{1}/_{2}$; D = $-x - {}^{1}/_{2}, y, -z + {}^{1}/_{2}$; E = $-x, -y + {}^{3}/_{2}, z$; F = $x, -y + {}^{1}/_{2}, z$; G = $-x, -y + {}^{1}/_{2}, z$. (b) Chain-based metal–organic layer. (c) Packing diagram showing the 1D rhombic channels through the layers and the interlayer interactions (represented by dashed lines).

3.570(1) Å for **2**, and the M–N–M angles for the azide bridges are 112.1(3) and 115.7(2)°, respectively. Adjacent MN_2O_4 octahedra along the chain share corners (the bridging N1 atoms) and are slanted with respect to each other, with the dihedral angles between the [MO_4] equatorial planes being 58° for **1** and 55° for **2**.

The formally anionic $[M(N_3)(OCO)_2]_n$ chains are charge-compensated and interlinked by the cationic *N*-benzylpyridinium backbone of the ligand to produce a 2D coordination layer parallel to the *ab* plane (Figure 1b). The nearest interchain M···M distance spanned by L^- is equal to the *b* dimension of the unit cell [13.692(3) Å for **1** and 13.503(4) Å for **2**]. The L^- ligand is imposed with crystallographic C_{2v} symmetry, so the pyridine and benzene rings are crystallographically indistinguishable, with C5 and N4 residing at the same site with equal occupancies. Along the *a* direction, the V-shaped L^- ligands hump alternately up and down from the layer, resulting in 1D rhombic channels running through the layer between neighboring chains (Figure 1c). The channels are filled by heavily disordered water molecules. The layer has highly corrugated surfaces for the layer, with metal ions at the bottom of the grooves and methylene groups at the top of the ridges. The azide ions stick out from the bottom of the grooves. In the lattice, the parallel layers are closely packed in an offset fashion, with the ridges from one layer inserting into the grooves of neighboring layers (Figure 1c). The interlayer separation is equal to $c/2$, and the nearest interlayer M···M distances are 11.391(2) Å for **1** and 11.374(3) Å for **2**. Two types of interactions are operative between layers. One is the face-to-face $\pi-\pi$ interaction between the parallel aromatic rings (benzene/pyridyl) from different layers, with the center-to-center and interplanar distances respectively 3.442(3) and 3.435(5) Å for **1** and 3.413(1) and 3.413(5) Å for **2**. The other interlayer interactions are weak C–H···N hydrogen bonds. Each N3 atom (the uncoordinated terminal atom of azide) from one layer interacts with six C–H groups from another layer, including two equivalent methylene C6–H groups and four equivalent aromatic C4–H groups) with H···N = 2.79–2.89 Å, C···N = 3.65–3.74 Å, and C–H···N = 146–155°.

Failing to obtain crystals suitable for single-crystal crystallography, we were unable to determine the structure of **3**, but the PXRD pattern of **3** is in good agreement with that of **2**, with only minor shifts in peak positions, indicating that **3** is isomorphous with **2**. The Pawley refinements[12] of the reflections of **3** in the same space group led to good agreements, and the cell parameters obtained are a = 7.065(1) Å, b = 13.450(2) Å, c = 18.382 Å, and V = 1746.7(2) Å^3. The *a* dimension and the cell volume of these compounds decrease in the order **1** > **2** > **3**, consistent with the decrease of the ionic radius in the order Mn^{II} > Co^{II} > Ni^{II}.

Magnetic Properties. The three isomorphous compounds show distinct magnetic properties owing to the different spin carriers.

Compound ***1***. The temperature dependence of the molar magnetic susceptibility (χ) of **1** in the range of 2–300 K is shown in Figure 2. The χT value at 300 K is 3.84 emu K mol^{-1},

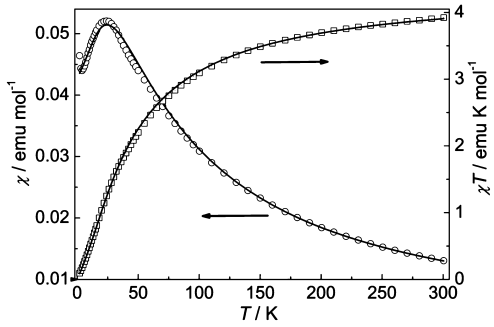

Figure 2. Temperature dependence of χ (molar magnetic susceptibility) and χT for **1** at 1 kOe. The solid lines present the best fit to the Fisher model.

lower than the spin-only value (4.375 emu K mol^{-1}) for magnetically isolated high-spin Mn^{II} ions (S = ${}^{5}/_{2}$). Upon cooling, the χT value decreases monotonically, while the χ value shows a broad maximum (0.052 emu mol^{-1}) at 24 K, with a slight increase below 4 K. The data above 110 K obey the Curie–Weiss law with C = 4.49 emu K mol^{-1} and θ = −43.7 K. The behaviors are typical of AF interactions between Mn^{II} ions.

dx.doi.org/10.1021/ic5014279 | Inorg. Chem. 2014, 53, 9306–9314

Table 2. Structural and Magnetic Parameters for the $(\mu\text{-}1,1\text{-}N_3)(\mu\text{-}1,3\text{-}COO)_2$ Bridges in Mn^{II} Compounds

complex[a]	Mn−N (Å)	Mn−O (Å)	Mn−N−Mn (deg)	τ (deg)[c]	Mn···Mn (Å)	J (cm^{-1})	ref
$[Mn_2(IM2\text{-}py)_2(N_3)_2(OAc)_2]_n \cdot n$EtOH (**I**)	2.24	2.13	106.8	9.1	3.591	−10.1	17a
$[Mn_3(ina)_2(pa)_2(N3)_2]_n$ (**II**)	2.18	2.18	109.9	21.6	3.569	−6.2	17b
$[Mn(L^1)_{0.5}(N_3)(OAc)]_n \cdot 3nH_2O$ (**III**)	2.21	2.18	110	20.5	3.612	−4.5	17c
$[Mn(L^2)(N_3)]_n(ClO_4)_n \cdot 0.5nH_2O$ (**IV**)[b]	A: 2.21	2.18	111.1	36.6	3.641	−4.27	10c
	B: 2.23	2.2	117.4	43.6	3.814	−1.19	
$Mn(L^3)(N_3)]_n(ClO_4)_n \cdot 0.5nH_2O$ (**V**)	2.23	2.18	111.1	39	3.68	−3.0	10b
$[[M(L)(N_3)]_n \cdot 3nH_2O$ (**1**)	2.22	2.17	112.1	10.7	3.675	−3.98	this work
$[Mn(S,S\text{-}L^5)(N_3)]_n \cdot 0.5nCH_3OH$ (**VI**)	2.27	2.169	115.2	26.6	3.827	−2.08	17d
$[Mn_3(R,S\text{-}L^5)_2(N_3)_4(H_2O)_2]_n$ (**VII**)	2.22	2.163	115.3	21.6	3.756	−2.08	17d
$[Mn(L^2)(N_3)]_{2n}[Mn(N_3)_4(H_2O)_2]_n \cdot 2nH_2O$ (**VIII**)	2.23	2.17	117	33.2	3.811	−1.02	10c
$[Mn(L^4)(N_3)]_n$ (**IX**)	2.3	2.164	117.9	16.9	3.94	−2.07	17d
$[Mn(cmpc)(N_3)]_n \cdot nH_2O$ (**X**)	2.18	2.15	120.7	17.8	3.783	−1.93	11e

[a] IM2-py = 4,4,5,5-tetramethyl-2-(2′-pyridyl)imidazolin-1-oxyl, pa = picolinate, ina = isonicotinate, L^1 = 1,4-bis(4-carboxylatopyridinium-1-methylene)benzene, L^2 = 1,3-bis(4-carboxylatopyridinium)propane, cmpc = 1-carboxylatomethylpyridinium-4-carboxylate, L^3 = 1,3-bis(3-carboxylatopyridinium)propane), L^4 = 1,3-bis(carboxylatomethyl)imidazolium, L^5 = 1,3-bis(1-carboxylatoethyl)imidazolium, and L^- = 1-(4-carboxylatobenzyl)pyridinium)-4-carboxylate. [b] This compound contains two sets (A and B) of $(\mu\text{-}1,1\text{-}N_3)(\mu\text{-}1,3\text{-}COO)_2$ bridges with distinct structural parameters. [c] The average Mn−O−C−O torsion angle for carboxylate bridges.

The slight increase of χ below 4 K could be attributed to the presence of a paramagnetic impurity.

According to the structural data, compounds **1**−**3** can magnetically be handled as infinite uniform chains in which magnetic coupling is mediated through triple $(\mu\text{-}1,1\text{-}N_3)(\mu\text{-}1,3\text{-}COO)_2$ bridges. The interchain magnetic interactions through the long organic ligand should be negligible because the sp^3 methyl group in the ligand destroys the conjugated system and only weak dipole−dipole interaction is possible between chains. For **1**, the intrachain interaction (J) can be evaluated using the classical spin expression derived by Fisher for isotropic Heisenberg chains ($H = -J\sum S_iS_{i+1}$):[16]

$$\chi_{chain} = [Ng^2\beta^2S(S+1)/3kT][(1+u)/(1-u)] \quad (1)$$

where u is the well-known Langevin function defined as $u = \coth[JS(S+1)/kT] - kT/[JS(S+1)]$ with $S = {}^5/_2$. The best fit of the experimental data to the expression leads to $J = -3.98$ cm^{-1} with $g = 1.98$.

The isothermal magnetization of **1** measured at 2.0 K increases slowly with the applied magnetic field and reaches a value of 0.83 Nβ at 50 kOe (Figure S2 in the SI), which is far below the saturation value (5 Nβ for $S = {}^5/_2$ and $g = 2.00$). The behavior confirms the AF coupling between Mn^{II} ions.

The $(\mu\text{-}1,1\text{-}N_3)(\mu\text{-}1,3\text{-}COO)_2$ bridging moiety has been observed in some Mn^{II} compounds reported elsewhere.[10b,c,11e,17] The compounds with available data of magnetic exchange are collected in Table 2, which also includes relevant structural data. Most (**III**−**X** and **1**) of these compounds are derived from pyridinium- or imidazolium-based zwitterionic carboxylate ligands. **I** is a 1D Mn^{II} radical complex with alternating $(\mu\text{-}1,1\text{-}N_3)(\mu\text{-}1,3\text{-}COO)_2$ and $\mu\text{-}1,3\text{-}N_3$ bridges, **II** contains a chain with alternating $(\mu\text{-}1,1\text{-}N_3)(\mu\text{-}1,3\text{-}COO)_2$ and $(\mu\text{-}O)_2$ bridges, and in **VII**, $(\mu\text{-}1,1\text{-}N_3)(\mu\text{-}1,3\text{-}COO)_2$-bridged trinuclear units are interlinked into 2D layers by $\mu\text{-}1,3\text{-}N_3$ bridges. All of the rest contain the chains with only $(\mu\text{-}1,1\text{-}N_3)(\mu\text{-}1,3\text{-}COO)_2$ bridges, although the dimensionality and interchain connecting topology are different. Whatever the extended structures, the $(\mu\text{-}1,1\text{-}N_3)(\mu\text{-}1,3\text{-}COO)_2$ bridging moiety seems to always induce AF coupling between Mn^{II} ions, with the J parameters in the range from −1 to −10 cm^{-1}. It is well-known that 1,1-azide usually induces FO coupling between metal ions (exceptions are the Cu^{II} species with large Cu−N−Cu angles),[7a,18] while *syn,syn*-carboxylate is an almost universal AF pathway.[19] The overall AF nature of the mixed pathways could be because the carboxylate pathway predominates over the azide one in Mn^{II} compounds. The magnitude of the AF coupling could be influenced by the structural parameters of both bridges, such as the Mn−N/O bond distances, the Mn−N−Mn angle of the azide bridge, and also the angular parameters of the carboxylate bridge. A close inspection into the data in Table 2 indicates that the most relevant parameter seems to be the Mn−N−Mn angle. As can be seen from the plot of J against Mn−N−Mn (Figure 3), the

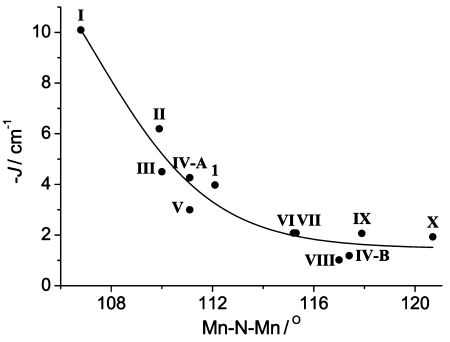

Figure 3. Correlation of the AF coupling through $(\mu\text{-}1,1\text{-}N_3)(\mu\text{-}1,3\text{-}COO)_2$ bridges to the Mn−N−Mn angle for the compounds listed in Table 2. The solid line is just a guide for the eye.

general trend is that the larger the bridging angle, the weaker the AF coupling. The trend is more evident in the small angle range (106−111°). The angular dependence is consistent with that for the azide-only bridge between Mn^{II} ions. Both experimental and theoretical studies have demonstrated that the FO coupling through double 1,1-azide bridges increases with the Mn−N−Mn angle.[18a,20] With this in mind, we can assume that the decrease of the AF coupling through $(\mu\text{-}1,1\text{-}N_3)(\mu\text{-}1,3\text{-}COO)_2$ with increasing Mn−N−Mn is due to the increase of the FO contribution from the azide pathway.

As can be seen from Figure 3, there are some significant deviations from the general trend. For example, the lowest $|J|$ value observed is not for compound **X**, which has the largest Mn−N−Mn angle (120.7°), but for compound **VIII** and bridge

dx.doi.org/10.1021/ic5014279 | Inorg. Chem. 2014, 53, 9306−9314

set B in **IV**, which have smaller angles (~117°). The deviations can be justified by the variations in other parameters. The interaction through the carboxylate pathway is strongly influenced by the out-of-plane distortion of the M−O−C−O−M moiety from the ideal coplanar syn,syn coordination mode.[19a] The overall distortion in these compounds may be roughly represented by the average Mn−O−C−O torsion angle (τ) for the two carboxylate bridges (Table 2). A large distortion will disfavor the interaction. Thus, the small $|J|$ values for compound **VIIII** and bridge set B in **IV** can be related to their large τ angles (>33°). For comparison, **X** and **IX** have τ < 18°. Similarly, the large τ angle (39°) for **V** may be responsible for its smaller $|J|$ value compared with **1** and **III**. Of all of these compounds, **I** has the smallest Mn−N−Mn and τ angles, consistent with its exceptionally large $|J|$ value. In these compounds, the influence of the bond distances is less apparent than the angular dependence. Nevertheless, the higher $|J|$ value of **II** compared with **III** may be due to its shorter Mn−N/O distances (the two compounds are similar in Mn−N−Mn and τ angles).

Compound 2. For this compound, the room-temperature χT value (3.38 emu K mol^{-1}) per Co^{II} ion is much larger than the spin-only value (1.875 emu K mol^{-1} for $S = {}^3/_2$ with $g = 2.00$), indicating the significant orbital contribution typical of the orbitally degenerate octahedral Co^{II}-^{4}T$_{1g}$ term. As the temperature is lowered, the susceptibility increases continuously, while the χT product increases to a maximum value of 68.6 emu K mol^{-1} at 7.0 K (for data measured at 1 kOe) and then decreases rapidly upon further cooling (Figure 4). The fit of the data

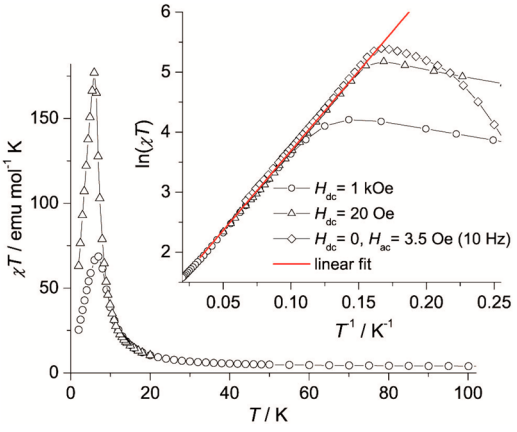

Figure 4. Temperature dependence of χT for **2** measured at 1 kOe (the featureless part above 100 K is omitted to better show the low-temperature part) and 20 Oe. Inset: ln(χT) versus $1/T$ plots. The red line represents the linear fit in the region between 8 and 32 K.

above 40 K to the Curie−Weiss law led to C = 3.19 emu K mol^{-1} and θ = 18.3 K. These behaviors evidently indicate that the Co^{II} compound shows intrachain FO coupling through the triple (μ-1,1-N$_3$)(μ-1,3-COO)$_2$ bridges and that the coupling is strong enough to overcome the thermal effect of the orbital contribution. The decrease of χT below 7.0 K may be due to (i) the effect of the applied magnetic field, (ii) weak interchain AF interactions, and/or (iii) the finite-size effect that operates when the divergence of the correlation length along the chain is suppressed by naturally occurring defects.[21] The involvement of the field effect is evidenced by the observation that the χT maximum increases to 176 emu K mol^{-1} and shifts to a lower temperature (5.9 K) for the data measured at a lower field of 20 Oe (Figure 4). Such field-dependent behavior is common for FO systems. The finite-size effect itself leads to saturation (not decrease) of χT at low temperature, but its combination with weak AF interactions between chain segments can lead to a decrease in χT.[22]

Since the unquenched orbital momentum and the consequent spin−orbital coupling intrinsic to octahedral Co^{II} impart strong magnetic anisotropy to the chain in **2**, the isotropic classical spin model used for **1** is not valid for **2**. It is well-known that the correlation length (ξ) of a 1D FO chain with uniaxial anisotropy diverges exponentially with temperature: $\xi \propto \chi T \approx C \exp(\Delta_\xi/kT)$ (where Δ_ξ is the energy cost to create a domain wall along the chain and χ is the zero-field susceptibility),[5a,b] which corresponds to a linear variation of ln(χT) with $1/T$. For **2**, the ln(χT) versus $1/T$ plot at 1 kOe (Figure 4, inset) shows a linear region between 10 and 32 K. The linear region extends to 6.9 K under a lower direct-current (dc) field of 20 Oe and further to 6.4 K for the in-phase alternating-current (ac) susceptibility data (χ') obtained under zero dc field (Figure 4, inset). The fitting results of the linear regions for these different data sets are very similar, and the average values are Δ_ξ/k = 26.3 K and C = 2.77 emu K mol^{-1}. The scaling treatments clearly indicate the uniaxial anisotropic character of the 1D FO system in **2**. Assuming the Co^{II} system at low temperature to be an Ising chain with $S_{eff} = {}^1/_2$, Δ_ξ is related to the magnetic exchange parameter J by $\Delta_\xi = 2JS_{eff}^2$ (based on Hamiltonian $H = -JS_{eff}^2\sum\sigma_i\sigma_{i+1}$ [$\sigma_i = \pm 1$)] and C is related to $g_\parallel$ by $C = Ng_\parallel^2\beta^2S_{eff}^2/3k$.[5b,23] With these equations, we have J/k = 52.6 K (J = 36.6 cm^{-1}) and $g_\parallel$ = 9.42.

The isothermal magnetization of **2** was measured from 0 to 50 kOe at 2 K (Figure 5). The very rapid rise of magnetization

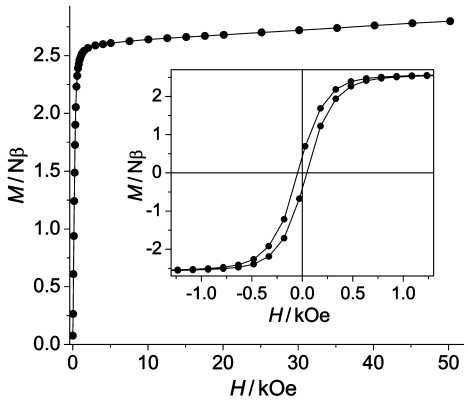

Figure 5. Isothermal magnetization curve of **2** at 2 K. The inset shows the hysteresis loop at 2 K. The lines are a guide for the eye.

in the low-field region from 0 to 1.5 kOe confirms the presence of FO coupling between Co^{II} ions. In the high-field region, the magnetization increases slowly and quasi-linearly, and the increase seems to continue above 50 kOe, which is consistent with the presence of magnetic anisotropy.[5a,24] Hysteresis measurements at 2 K (Figure 5, inset) gave a small coercive field (45 Oe) and a small remnant magnetization (0.42 Nβ), suggesting soft-magnet-like irreversible magnetization behaviors. The field-cooled (FC) and zero-field-cooled (ZFC) magnetization measurements were also performed at 20 Oe (Figure S3 in the SI). The divergence between FC and ZFC data below 5.6 K also indicates a magnet-like irreversibility.

To gain insight into the origin of the magnet-like behaviors, temperature (T)- and frequency (f)-dependent ac susceptibil-

dx.doi.org/10.1021/ic5014279 | Inorg. Chem. 2014, 53, 9306−9314

ities were measured under zero dc field with a driving ac field of 3.5 Oe. As shown in Figures 6 and S4 in the SI, the out-of-

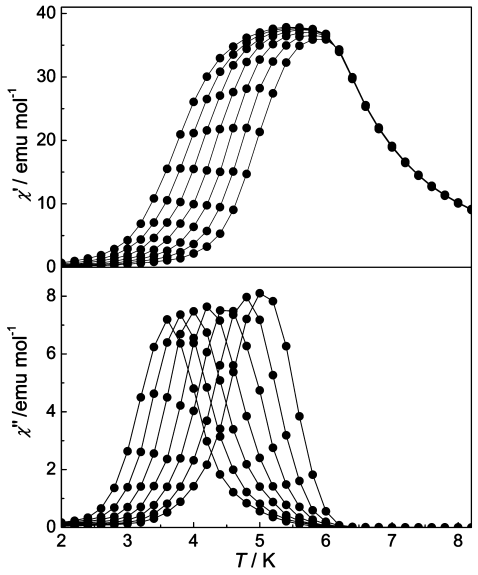

Figure 6. Thermal dependence of ac magnetic susceptibilities of **2** measured at zero dc field with a driving ac field (3.5 Oe) at different frequencies (from left to right: 1, 3, 10, 32, 100, 320, and 997 Hz).

phase signal (χ'') appears below 6.2 K and both χ' and χ'' are strongly frequency-dependent, with the $\chi''(T)$ [$\chi''(f)$] maximum shifting toward high temperature (frequency) as the frequency (temperature) is increased. The behaviors are indicative of slow relaxation of magnetization. The parameter measuring the frequency dependence, $\varphi = (\Delta T_p/T_p)/\Delta(\log f)$ [T_p is the temperature at which a maximum appears in the $\chi''(T)$ plot], was estimated to be 0.10. A similar parameter, $\varphi' = (\Delta T/T)/\Delta(\log f_p) = 0.11$ [f_p is the frequency at which a maximum appears in the $\chi''(f)$ plot], was estimated from the $\chi''(f)$ plot. These values are out of the range for canonical spin glasses ($\varphi \leq 0.08$) but in the range for superparamagnets,[25] including SCMs.[6c,8a,b,26] The relaxation times τ at different temperatures were obtained from the $\chi''(f)$ data, $\tau = 1/(2\pi f_p)$. The data obey the Arrhenius equation $\tau = \tau_0 \exp(\Delta_\tau/kT)$ with $\Delta_\tau = 86.4$ K and $\tau_0 = 1.1 \times 10^{-11}$ s (Figure S5 in the SI). The physically reasonable parameters suggest that the slow relaxation of magnetization in **2** is a thermally activated process ($\Delta\tau$ is the energy barrier to reverse the magnetization). The Δ_τ and τ_0 values lie in the usual range for superparamagnets including SCMs.[6a] Because $\Delta_\tau > 2\Delta_\xi$, the spin flip in the chain experiences an anisotropic barrier energy in addition to the barrier related to magnetic exchange between neighboring spins. Assuming that the relaxation is activated inside the chain ("volume" excitation), for which $\Delta_\tau = 2\Delta_\xi + \Delta_A$,[5a,b] the anisotropic barrier can be deduced to be $\Delta_A/k \approx 34$ K. Because Δ_A is larger than Δ_ξ, the compound has narrow domain walls, as expected for an Ising chain.

Using the frequency-dependent isothermal ac data of **2**, we obtained semicircular $\chi''-\chi'$ curves (Cole–Cole diagram; Figure 7). The fit of the data to a general Debye model[27] gave α values in the range 0.35–0.41. The values lie within the range reported for known SCMs and indicate a distribution of the relaxation time.

This compound is the third compound containing uniform Co^{II} chains with $(\mu\text{-}1,1\text{-}N_3)(\mu\text{-}1,3\text{-}COO)_2$ bridges. Some

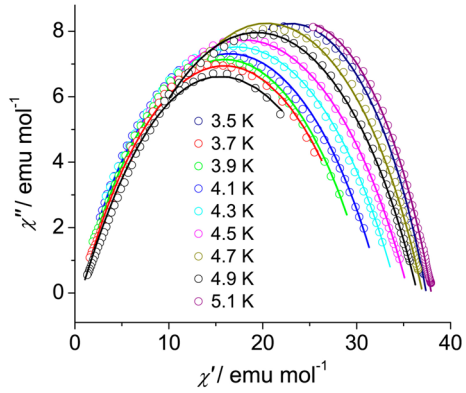

Figure 7. Cole–Cole diagram for **2**, plotted using $\chi'(f)$ and $\chi''(f)$ at different temperatures. The solid lines represent the fits to a general Debye model.

structural and magnetic data of the known compounds are compared in Table 3. The previous compounds **XI** and **XII** exhibit chain-based 2D or 3D metal–organic frameworks with topologies different from that of **2**.[11d,f] They are also derived from zwitterionic dicarboxylate ligands, show intrachain FO coupling through the mixed azide and carboxylate bridges, and behave as SCMs. The FO coupling indicates that the FO pathway (azide) predominates over the AF pathway (carboxylate) in these Co^{II} compounds, in contrast to the situation in the Mn^{II} analogues (vide supra). Of these Co^{II} compounds, **2** has the highest blocking temperature (T_B), associated with the highest Δ_τ and Δ_A energies but the lowest Δ_ξ energy.

The Δ_ξ energy is related to the intrachain FO coupling. As mentioned above, the FO coupling via 1,1-azide between Mn^{II} ions increases as the Mn–N–Mn angle increases, and the AF coupling via 1,3-carboxylate decreases as the Mn–O–C–O torsion angle increases. The Co^{II} compounds with $(\mu\text{-}1,1\text{-}N_3)(\mu\text{-}1,3\text{-}COO)_2$ bridges seems to have similar angular dependence. Here, both the Co–N–Co angle and the average Co–O–C–O angle increase in the order **2** < **XI** < **XII**, and then the FO contribution via 1,1-azide increases in the same order and the AF contribution via 1,3-carboxylate decreases in the order **2** > **XI** > **XII**. Thus, the overall FO coupling through the mixed bridges increases in the order **2** < **XI** < **XII**, consistent with the trend in the Δ_ξ energy. The slight decrease from **2** through **XI** to **XII** in Co–N distances may also contribute to the increase of the FO coupling. On the basis of only three compounds, it is difficult to determine which factor is the most important, and the correlations need to be confirmed by extended studies.

The reason that **2** exhibits a significantly higher Δ_A energy than **XI** and **XII** is more complicated. If single-ion anisotropy is assumed, Δ_A should be related to the local environment of Co^{II}. The Co^{II} ions in all of these compounds adopt the trans-octahedral $[N_2O_4]$ geometry with tetragonal distortion. Differently, the elongation is along an O–Co–O axis in **XI** and **XII** but along the N–Co–N axis in **2**. The relationship between the anisotropy energy and the different distortions is open to further studies. Control of Δ_A has been a difficult challenge in the design of SCMs.

As to the relaxation barrier (Δ_τ), the relatively high value of **2** is not only related to the high Δ_A energy but may also be due to the fact that slow relaxation occurs inside "infinite" chains ($\Delta_\tau = 2\Delta_\xi + \Delta_A$). Relaxation in **XI** and **XII** occurs in the "finite-chain" regime ($\Delta_\tau = \Delta_\xi + \Delta_A$), where growth of the correlation length

dx.doi.org/10.1021/ic5014279 | Inorg. Chem. 2014, 53, 9306–9314

Table 3. Structural and Magnetic Parameters for Co^{II} SCMs with (μ-1,1-N_3)(μ-1,3-COO)$_2$ Bridges

complex[a]	Co−N (Å)	Co−O (Å)	Co−N−Co (deg)	τ (deg)[b]	Co···Co (Å)	Δ_ξ/k (K)	Δ_τ/k (K)	Δ_A/k (K)	T_B (K)[c]	ref
$[Co(L)(N_3)]_n \cdot 3nH_2O$ (**2**)	2.11	2.09	115.7	10.8	3.570	26	86	34	5.0	this work
$[Co(cmpc)(N_3)]_n \cdot nH_2O$ (**XI**)	2.10	2.10, 2.12	120.7	17.5	3.656	30	50	20	3.9	11f
$[Co(L^6)(N_3)]_n \cdot nH_2O$ (**XII**)	2.09	2.10, 2.12	122.2	27.0	3.659	39	49	10	3.6	11d

[a] L^- = 1-(4-carboxylatobenzyl)pyridinium)-4-carboxylate, cmpc = 1-carboxylatomethylpyridinium-4-carboxylate, and L^6 = 1-carboxymethylpyridinium-4-benzoate. [b] Taken as the temperature of the χ'' versus T curve at 1 kHz. [c] Average Co−O−C−O torsion angle for the carboxylate bridges.

is limited by naturally occurring defects and spin flip begins at the end of a chain ("surface" excitation). Interestingly, the comparisons of these compounds indicate a dilemma in the design of SCMs. On the one hand, higher Δ_ξ (associated with stronger intrachain coupling) is desirable for the enhancement of Δ_τ and T_B. On the other hand, with higher Δ_ξ, growth of the correlation length upon cooling is more rapid, and the finite-size effect may be relevant at higher temperature, suppressing the volume excitation.

Compound **3**. The χT value of this compound at room temperature is about 1.45 emu K mol^{-1}, larger than the spin-only value (1.00 emu K mol^{-1}) expected for a magnetically isolated Ni^{II} ion. The relatively large difference is not only because of the high g value of single octahedral Ni^{II} ions but also due to possible FO coupling between Ni^{II} ions. The general temperature-dependent behavior of the susceptibility is similar to that of compound **2**. Upon cooling, χ increases monotonically, while the χT product shows a maximum of about 20.0 emu K mol^{-1} at 6.1 K (Figure 8). The data above 90 K obey the Curie−Weiss law with C = 1.17 emu K mol^{-1} and θ = 51.4 K. The behaviors evidently confirm the occurrence of FO coupling between Ni^{II} ions.

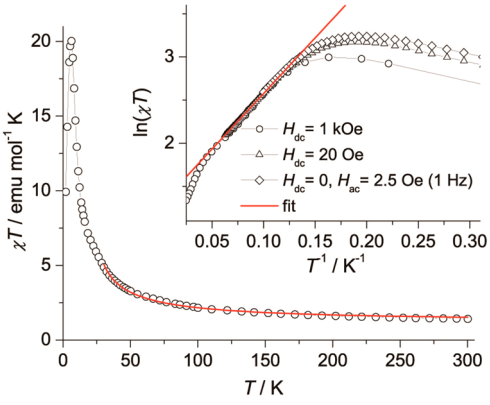

Figure 8. Temperature dependence of χT for **3** measured at 1 kOe. Inset: ln(χT) versus 1/T plots. The red lines represent the fits (see the text).

Isothermal magnetization measurements were performed at 2.0 K (Figure S6 in the SI). The rapid increase of magnetization with the field confirms the FO coupling between Ni^{II} ions. No hysteresis was detected when the field was cycled between ±50 kOe. The ZFC and FC magnetizations measured at 20 Oe show no appreciable divergence above 2 K.

To evaluate the magnitude of the coupling, the susceptibility data were analyzed using the polynomial expression for FO Ni^{II} chains ($H = -J\sum S_i S_{i+1}$):[10a,28]

$$\chi = (2N\beta^2 g^2/3kT)(AX^3 + BX^2 + CX + 1)/(DX^2 + EX + 1) \quad (2)$$

where $X = J/kT$ and the coefficients are A = 0.14709, B = −0.788967, C = 0.866426, D = 0.096573, and E = −0.624929. The best fit of the data above 30 K produced J = 35.3 cm^{-1} (J/k = 50.8 K) with g = 2.21. Considering that Ni^{II} (S = 1) experiences zero-field splitting (ZFS), the FO Ni^{II} chain can be better described as an anisotropic Heisenberg chain in which single-ion anisotropy is characterized by an axial ZFS parameter (D). The susceptibility data were also fitted to the expression proposed by de Neef,[29] which includes the D parameter, leading to J = 31.8 cm^{-1} (J/k = 45.7 K) and D = −2.1 cm^{-1} (D/k = −3.0 K) with g = 2.29. The D value lies within the usual range (several Kelvins) for Ni^{II} complexes. It should be noted that the fit using de Neef's expression is insensitive to the variation of D, as indicated in previous studies. The above value is only a rough estimation. If assuming D = 0, the best fit of de Neef's expression led to J = 30.6 cm^{-1} (J/k = 44.0 K) with g = 2.29.

It has been theoretically argued that the expression $\xi \propto \chi T \approx C \exp(\Delta_\xi/kT)$ applies for any anisotropic chain with $D < 0$ when the correlation length is much larger than the width of the domain wall.[5a,30] Accordingly, we plotted ln(χT) against 1/T for **2** using the data obtained under 1 kOe, 20 Oe, and zero dc field. A linear region from 22 to 8 K is evident, with the slope giving Δ_ξ/k = 13 K. This indicates that the Ni^{II} ion in **2** has a negative D value (i.e., uniaxial anisotropy) and that the correlation length is much larger than the width of the domain wall at low temperature. Considering the above-obtained J values, it is evident that the equation $\Delta_\xi = 2JS^2$ (S = 1) is not valid here. The equation applies only for systems with large anisotropy ($|D/J| > {}^4/_3$). With weaker anisotropy, as for **2**, the width of the domain wall is large and its creation energy (Δ_ξ) shows a complex dependence on both J and D.[5d]

Thermal ac magnetic susceptibilities of **3** were measured under zero dc field with a driving ac field of 2.5 Oe oscillating at different frequencies (Figure 9). The imaginary signal at 1 kHz becomes nonzero at 2.6 K, below which the real and imaginary components show evident frequency dependence. No peaks in the imaginary signals were observed above 1.8 K (the lowest temperature available with the measurement system used). The behavior suggests the occurrence of slow relaxation of magnetization. Considering the FO coupling and the uniaxial anisotropy within the Ni^{II} chain, it is likely that the slow dynamics stems from the reversal of magnetization of individual chains, for which the activation energy is not high enough to block the magnetization above 1.8 K. However, the possibility of a spin-glass-like behavior cannot be precluded at this stage. The origin merits further investigation.

dx.doi.org/10.1021/ic5014279 | Inorg. Chem. 2014, 53, 9306−9314

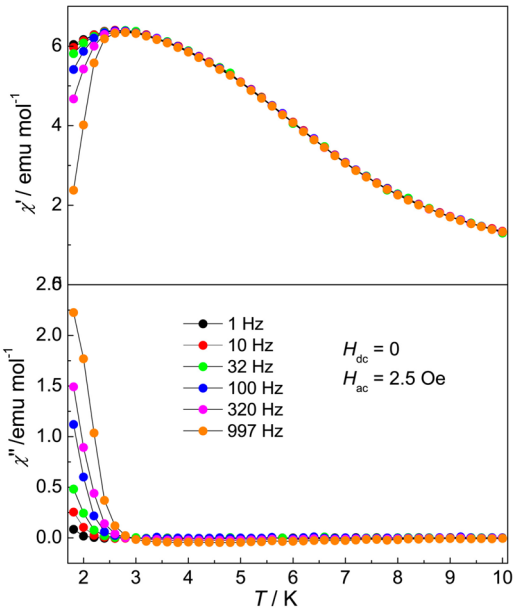

Figure 9. Thermal dependence of ac magnetic susceptibilities of **3** measured at different frequencies.

CONCLUSIONS

Three isomorphous 2D coordination polymers based on the chain with triple $(\mu\text{-}1,1\text{-}N_3)(\mu\text{-}1,3\text{-}COO)_2$ bridges have been synthesized from a new zwitterionic dicarboxylate ligand. It has been demonstrated that the magnetic properties depend strongly upon the nature of the metal center. First, the magnetic coupling through $(\mu\text{-}1,1\text{-}N_3)(\mu\text{-}1,3\text{-}COO)_2$ is AF in the Mn^{II} compound but FO in the Co^{II} and Ni^{II} analogues. Second, the FO systems show different magnetization dynamics depending on magnetic anisotropy. With strong anisotropy, the Co^{II} compound behaves as a SCM showing Glauber-type slow dynamics. It shows the highest blocking temperature among the known Co^{II} SCMs with similar bridges, associated with the highest Δ_τ and Δ_A energies but the lowest Δ_ξ energy. With weaker anisotropy, the Ni^{II} species shows slow relaxation of magnetization at much lower temperature. Magnetostructural analyses have indicated that the magnitude of the magnetic coupling can be correlated to the M−N−M angle of the azide bridge and the average M−O−C−O torsion angle of the carboxylate bridge. With the increase of these parameters, the AF coupling for Mn^{II} decreases while the FO coupling for Co^{II} increases. The energetic differences between the Co^{II} SCM and previous analogues have also been related to structural differences. This work also demonstrates the efficiency of the mixed azide and carboxylate approach in generating 1D magnetic systems and FO SCMs. In addition, this series of isomorphous compounds offers the potential of investigating mixed-metal SCMs. Work along this line is underway.

ASSOCIATED CONTENT

Supporting Information

Crystallographic information for compounds **1** and **2** in CIF format and supplementary structural graphics. This material is available free of charge via the Internet at http://pubs.acs.org.

AUTHOR INFORMATION

Corresponding Author

*E-mail: eqgao@chem.ecnu.edu.cn.

Notes

The authors declare no competing financial interest.

ACKNOWLEDGMENTS

This work is supported by the National Natural Science Foundation of China (Grants 21173083 and 91022017) and the Research Fund for the Doctoral Program of Higher Education of China.

REFERENCES

(1) (a) Kahn, O. *Molecular Magnetism*; VCH: New York, 1993. (b) Miller, J. S.; Drillon, M. *Magnetism: Molecules to Materials*; Wiley-VCH: Weinheim, Germany, 2002−2005; Vols. *I*−*V*. (c) Wang, X. Y.; Avendano, C.; Dunbar, K. R. *Chem. Soc. Rev.* **2011**, *40*, 3213−3238. (d) Weng, D. F.; Wang, Z. M.; Gao, S. *Chem. Soc. Rev.* **2011**, *40*, 3157−3181.

(2) (a) Aubin, S. M. J.; Wemple, M. W.; Adams, D. M.; Tsai, H.-L.; Christou, G.; Hendrickson, D. N. *J. Am. Chem. Soc.* **1996**, *118*, 7746−7754. (b) Gatteschi, D.; Sessoli, R. *Angew. Chem., Int. Ed.* **2003**, *42*, 268−297. (c) Arnold, P. L. *Nat. Chem.* **2012**, *4*, 967−969. (d) Habib, F.; Murugesu, M. *Chem. Soc. Rev.* **2013**, *42*, 3278−3288. (e) Zhang, P.; Guo, Y.-N.; Tang, J. *Coord. Chem. Rev.* **2013**, *257*, 1728−1763. (f) Ungur, L.; Lin, S.-Y.; Tang, J.; Chibotaru, L. F. *Chem. Soc. Rev.* **2014**, DOI: 10.1039/c1034cs00095a.

(3) (a) Guo, Y. N.; Xu, G. F.; Gamez, P.; Zhao, L.; Lin, S. Y.; Deng, R. P.; Tang, J. K.; Zhang, H. J. *J. Am. Chem. Soc.* **2010**, *132*, 8538−8539. (b) Guo, Y.-N.; Xu, G.-F.; Wernsdorfer, W.; Ungur, L.; Guo, Y.; Tang, J.; Zhang, H.-J.; Chibotaru, L. F.; Powell, A. K. *J. Am. Chem. Soc.* **2011**, *133*, 11948−11951. (c) Lin, S.-Y.; Wernsdorfer, W.; Ungur, L.; Powell, A. K.; Guo, Y.-N.; Tang, J.; Zhao, L.; Chibotaru, L. F.; Zhang, H.-J. *Angew. Chem., Int. Ed.* **2012**, *51*, 12767−12771. (d) Zhang, P.; Zhang, L.; Wang, C.; Xue, S.; Lin, S.-Y.; Tang, J. *J. Am. Chem. Soc.* **2014**, *136*, 4484−4487. (e) Zhao, L.; Wu, J.; Ke, H.; Tang, J. *Inorg. Chem.* **2014**, *53*, 3519−3525.

(4) (a) Caneschi, A.; Gatteschi, D.; Lalioti, N.; Sangregorio, C.; Sessoli, R.; Venturi, G.; Vindigni, A.; Rettori, A.; Pini, M. G.; Novak, M. A. *Angew. Chem., Int. Ed.* **2001**, *40*, 1760−1763. (b) Clérac, R.; Miyasaka, H.; Yamashita, M.; Coulon, C. *J. Am. Chem. Soc.* **2002**, *124*, 12837−12844.

(5) (a) Coulon, C.; Miyasaka, H.; Clérac, R. *Struct. Bonding (Berlin)* **2006**, *122*, 163−206. (b) Bogani, L.; Vindigni, A.; Sessoli, R.; Gatteschi, D. *J. Mater. Chem.* **2008**, *18*, 4750−4758. (c) Zhang, W.-X.; Ishikawa, R.; Breedlove, B.; Yamashita, M. *RSC Adv.* **2013**, *3*, 3772−3798. (d) Miyasaka, H.; Julve, M.; Yamashita, M.; Clerac, R. *Inorg. Chem.* **2009**, *48*, 3420−3437.

(6) (a) Sun, H.-L.; Wang, Z.-M.; Gao, S. *Coord. Chem. Rev.* **2010**, *254*, 1081−1100. (b) Liu, T.; Zheng, H.; Kang, S.; Shiota, Y.; Hayami, S.; Mito, M.; Sato, O.; Yoshizawa, K.; Kanegawa, S.; Duan, C. *Nat. Commun.* **2013**, *4*, 2826. (c) Mougel, V.; Chatelain, L.; Hermle, J.; Caciuffo, R.; Colineau, E.; Tuna, F.; Magnani, N.; de, G. A.; Pecaut, J.; Mazzanti, M. *Angew. Chem., Int. Ed.* **2014**, *53*, 819−823.

(7) (a) Ribas, J.; Escuer, A.; Monfort, M.; Vicente, R.; Cortes, R.; Lezama, L.; Rojo, T. *Coord. Chem. Rev.* **1999**, *193*−*5*, 1027−1068. (b) Wang, X. Y.; Wang, Z. M.; Gao, S. *Chem. Commun.* **2008**, 281−294. (c) Zeng, Y. F.; Hu, X.; Liu, F. C.; Bu, X. H. *Chem. Soc. Rev.* **2009**, *38*, 469−480. (d) Kurmoo, M. *Chem. Soc. Rev.* **2009**, *38*, 1353−1379. (e) Dechambenoit, P.; Long, J. R. *Chem. Soc. Rev.* **2011**, *40*, 3249−3265.

(8) (a) Liu, T. F.; Fu, D.; Gao, S.; Zhang, Y. Z.; Sun, H. L.; Su, G.; Liu, Y. J. *J. Am. Chem. Soc.* **2003**, *125*, 13976−13977. (b) Stamatatos, T. C.; Abboud, K. A.; Wernsdorfer, W.; Christou, G. *Inorg. Chem.* **2009**, *48*, 807−809. (c) Hu, B.-W.; Zhao, J.-P.; Yang, Q.; Zhang, X.-F.; Evangelisti, M.; Sanudo, E. C.; Bu, X.-H. *Dalton Trans.* **2010**, *39*, 11210−11217. (d) Li, Z. X.; Zeng, Y. F.; Ma, H.; Bu, X. H. *Chem. Commun.* **2010**, *46*, 8540−8542. (e) Song, X. Y.; Yang, P. P.; Mei, X. L.; Li, L. C.; Liao, D. Z. *Eur. J. Inorg. Chem.* **2010**, 1689−1695. (f) Yoon, J. H.; Lee, J. W.; Ryu, D. W.; Yoon, S. W.; Suh, B. J.; Kim, H. C.; Hong, C. S. *Chem.—Eur. J.* **2011**, *17*, 3028−3034. (g) Bhargavi, G.;

Rajasekharan, M. V.; Costes, J. P.; Tuchagues, J. P. *Dalton Trans.* **2013**, *42*, 8113−8123.
(9) (a) Li, X. J.; Wang, X. Y.; Gao, S.; Cao, R. *Inorg. Chem.* **2006**, *45*, 1508−1516. (b) Zheng, Y.-Z.; Tong, M.-L.; Zhang, W.-X.; Chen, X.-M. *Angew. Chem., Int. Ed.* **2006**, *45*, 6310−6314. (c) Zheng, Y. Z.; Xue, W.; Tong, M. L.; Chen, X. M.; Grandjean, F.; Long, G. J. *Inorg. Chem.* **2008**, *47*, 4077−4087. (d) Zheng, Y. Z.; Xue, W.; Tong, M. L.; Chen, X. M.; Zheng, S. L. *Inorg. Chem.* **2008**, *47*, 11202−11211. (e) Hu, S.; Yun, L.; Zheng, Y.-Z.; Lan, Y.-H.; Powell, A. K.; Tong, M.-L. *Dalton Trans.* **2009**, 1897−1900. (f) Liu, C. M.; Zhang, D. Q.; Zhu, D. B. *Inorg. Chem.* **2009**, *48*, 4980−4987. (g) Zheng, Y.-Z.; Xue, W.; Zhang, W.-X.; Tong, M.-L.; Chen, X.-M.; Grandjean, F.; Long, G. J.; Ng, S.-W.; Panissod, P.; Drillon, M. *Inorg. Chem.* **2009**, *48*, 2028−2042. (h) Zhang, S. Y.; Shi, W.; Lan, Y. H.; Xu, N.; Zhao, X. Q.; Powell, A. K.; Zhao, B.; Cheng, P.; Liao, D. Z.; Yan, S. P. *Chem. Commun.* **2011**, *47*, 2859−2861. (i) Zhang, W. X.; Shiga, T.; Miyasaka, H.; Yamashita, M. *J. Am. Chem. Soc.* **2012**, *134*, 6908−6911. (j) Zhao, J. P.; Yang, Q.; Liu, Z. Y.; Zhao, R.; Hu, B. W.; Du, M.; Chang, Z.; Bu, X. H. *Chem. Commun.* **2012**, *48*, 6568−6570.
(10) (a) Ma, Y.; Zhang, J.-Y.; Cheng, A.-L.; Sun, Q.; Gao, E.-Q.; Liu, C. M. *Inorg. Chem.* **2009**, *48*, 6142−6151. (b) Tian, C. Y.; Sun, W. W.; Jia, Q.-X.; Tian, H.; Gao, E.-Q. *Dalton Trans.* **2009**, 6109−6113. (c) Wang, Y.-Q.; Jia, Q.-X.; Wang, K.; Cheng, A.-L.; Gao, E.-Q. *Inorg. Chem.* **2010**, *49*, 1551−1560. (d) Ma, Y.; Bandeira, N. A. G.; Robert, V.; Gao, E.-Q. *Chem.—Eur. J.* **2011**, *17*, 1988−1998.
(11) (a) Jia, Q.-X.; Tian, H.; Zhang, J.-Y.; Gao, E.-Q. *Chem.—Eur. J.* **2011**, *17*, 1040−1051. (b) Li, X.-B.; Zhang, J.-Y.; Wang, Y.-Q.; Song, Y.; Gao, E.-Q. *Chem.—Eur. J.* **2011**, *17*, 13883−13891. (c) Wang, Y.-Q.; Sun, W.-W.; Wang, Z.-D.; Jia, Q.-X.; Gao, E.-Q.; Song, Y. *Chem. Commun.* **2011**, *47*, 6386−6388. (d) Zhang, X.-M.; Wang, Y.-Q.; Wang, K.; Gao, E.-Q.; Liu, C.-M. *Chem. Commun.* **2011**, *47*, 1815−1817. (e) Wang, Y.-Q.; Yue, Q.; Qi, Y.; Wang, K.; Sun, Q.; Gao, E.-Q. *Inorg. Chem.* **2013**, *52*, 4259−4268. (f) Wang, Y.-Q.; Cheng, A.-L.; Liu, P.-P.; Gao, E.-Q. *Chem. Commun.* **2013**, *49*, 6995−6997.
(12) (a) Pawley, G. S. *J. Appl. Crystallogr.* **1981**, *14*, 357−361. (b) *Materials Studio*, version 5.0.0; Accelrys Software Inc.: San Diego, CA, 2009.
(13) Wang, X.-B.; Dacres, J. E.; Yang, X.; Broadus, K. M.; Lis, L.; Wang, L.-S.; Kass, S. R. *J. Am. Chem. Soc.* **2003**, *125*, 296−304.
(14) Sheldrick, G. M. *SADABS, Program for Empirical Absorption Correction*; University of Göttingen: Göttingen, Germany, 1996.
(15) Sheldrick, G. M. *SHELXTL*; Bruker Analytical X-ray Instruments Inc.: Madison, WI, 1998.
(16) Fisher, M. E. *Am. J. Phys.* **1964**, *32*, 343−346.
(17) (a) Wang, L.; Liu, Z.; Zhang, C.; Liu, Z.; Liao, D.; Jiang, Z.; Yan, S. *Sci. China, Ser. B: Chem.* **2003**, *46*, 533−541. (b) Cheng, L.; Zhang, W.-X.; Ye, B.-H.; Lin, J.-B.; Chen, X.-M. *Eur. J. Inorg. Chem.* **2007**, *2007*, 2668−2676. (c) Wang, Y.-Q.; Sun, Q.; Yue, Q.; Cheng, A.-L.; Song, Y.; Gao, E.-Q. *Dalton Trans.* **2011**, *40*, 10966−10974. (d) Wang, X.; Li, X.-B.; Yan, R.-H.; Wang, Y.-Q.; Gao, E.-Q. *Dalton Trans.* **2013**, *42*, 10000−10010.
(18) (a) Gao, E.-Q.; Bai, S. Q.; Yue, Y. F.; Wang, Z. M.; Yan, C. H. *Inorg. Chem.* **2003**, *42*, 3642−3649. (b) Bai, S. Q.; Gao, E.-Q.; He, Z.; Fang, C. J.; Yue, Y. F.; Yan, C. H. *Eur. J. Inorg. Chem.* **2006**, 407−415.
(19) (a) Rodriguez-Fortea, A.; Alemany, P.; Alvarez, S.; Ruiz, E. *Chem.—Eur. J.* **2001**, *7*, 627−637. (b) Maji, T. K.; Sain, S.; Mostafa, G.; Lu, T.-H.; Ribas, J.; Monfort, M.; Chaudhuri, N. R. *Inorg. Chem.* **2003**, *42*, 709−716.
(20) (a) Ruiz, E.; Cano, J.; Alvarez, S.; Alemany, P. *J. Am. Chem. Soc.* **1998**, *120*, 11122−11129. (b) Yu, M. M.; Ni, Z. H.; Zhao, C. C.; Cui, A. L.; Kou, H. Z. *Eur. J. Inorg. Chem.* **2007**, 5670−5676. (c) Ni, Z. H.; Kou, H. Z.; Zheng, L.; Zhao, Y. H.; Zhang, L. F.; Wang, R. J.; Cui, A. L.; Sato, O. *Inorg. Chem.* **2005**, *44*, 4728−4736.
(21) (a) Bogani, L.; Caneschi, A.; Fedi, M.; Gatteschi, D.; Massi, M.; Novak, M. A.; Pini, M. G.; Rettori, A.; Sessoli, R.; Vindigni, A. *Phys. Rev. Lett.* **2004**, *92*, 207204. (b) Bogani, L.; Sessoli, R.; Pini, M. G.; Rettori, A.; Novak, M. A.; Rosa, P.; Massi, M.; Fedi, M. E.; Giuntini, L.; Caneschi, A.; Gatteschi, D. *Phys. Rev. B* **2005**, *72*, 064406.
(22) (a) Coulon, C.; Clerac, R.; Lecren, L.; Wernsdorfer, W.; Miyasaka, H. *Phys. Rev. B* **2004**, *69*, 132408. (b) Wang, Y.-Q.; Zhang, X.-M.; Li, X.-B.; Wang, B.-W.; Gao, E.-Q. *Inorg. Chem.* **2011**, *50*, 6314−6322.
(23) Ising, E. *Z. Phys.* **1925**, *31*, 253−258.
(24) Miyasaka, H.; Takayama, K.; Saitoh, A.; Furukawa, S.; Yamashita, M.; Clérac, R. *Chem.—Eur. J.* **2010**, *16*, 3656−3662.
(25) Mydosh, J. A. *Spin Glasses: An Experimental Introduction*; Taylor & Francis: London, 1993.
(26) (a) Yoon, J. H.; Ryu, D. W.; Kim, H. C.; Yoon, S. W.; Suh, B. J.; Hong, C. S. *Chem.—Eur. J.* **2009**, *15*, 3661−3665. (b) Coronado, E.; Galán-Mascarós, J. R.; Martí-Gastaldo, C. *J. Am. Chem. Soc.* **2008**, *130*, 14987−14989.
(27) (a) Cole, K. S.; Cole, R. H. *J. Chem. Phys.* **1941**, *9*, 341−351. (b) Aubin, S. M. J.; Sun, Z.; Pardi, L.; Krzystek, J.; Folting, K.; Brunel, L.-C.; Rheingold, A. L.; Christou, G.; Hendrickson, D. N. *Inorg. Chem.* **1999**, *38*, 5329−5340.
(28) Monfort, M.; Resino, I.; El Fallah, M. S.; Ribas, J.; Solans, X.; Font-Bardia, M.; Stoeckli-Evans, H. *Chem.—Eur. J.* **2001**, *7*, 280−287.
(29) (a) de Neef, T. Ph.D. Thesis, Eindhoven University, Eindhoven, The Netherlands, 1975. (b) Kou, H. Z.; Hishiya, S.; Sato, O. *Inorg. Chim. Acta* **2008**, *361*, 2396−2406.
(30) (a) Barbara, B. *J. Phys. (Paris)* **1973**, *34*, 1039−1046. (b) Barbara, B. *J. Magn. Magn. Mater.* **1994**, *129*, 79−86.